Pergamon

Acta mater. 49 (2001) 3609–3620

Acta MATERIALIA

www.elsevier.com/locate/actamat

# SHAPE MEMORY AND PSEUDOELASTIC BEHAVIOR OF 51.5%Ni–Ti SINGLE CRYSTALS IN SOLUTIONIZED AND OVERAGED STATE

**H. SEHITOGLU[1]†, J. JUN[1], X. ZHANG[1], I. KARAMAN[2], Y. CHUMLYAKOV[3], H. J. MAIER[4] and K. GALL[5]**

[1]University of Illinois, Department of Mechanical and Industrial Engineering, 1206 W. Green St, Urbana, IL 61801, USA, [2]Department of Mechanical Engineering, Texas A&M University, College Station, TX 77843, USA, [3]Siberian Physical–Technical Institute, Revolution Sq. 1, 634050, Tomsk, Russia, [4]University of Paderborn, Lehrstuhl f. Werkstoffkunde, D-33095 Paderborn, Germany and [5]Department of Mechanical Engineering, University of Colorado, Boulder, CO, 80309, USA

*( Received 6 February 2001; received in revised form 17 May 2001; accepted 17 May 2001 )*

**Abstract**—Deformation of nickel rich (51.5%Ni) Ni–Ti single crystals are investigated over a wide range of temperatures (77–440 K) and strain levels in compression as high as 9%. These alloys combine high strength with an unusually wide pseudoleasticity temperature interval (near 200 K) and can be exploited to suit specific applications. The slip deformation in [001] orientation can not occur due to the prevailing slip systems, as confirmed by transmission electron microscopy. Consequently, the [001] orientation exhibited pseudoleastic deformation at temperatures ranging from 77 to 283 K for the solutionized case and 273–440 K for the aged condition respectively. The critical transformation stress levels were in the range 800–1800 MPa for the solutionized case, and 200–1000 MPa for the aged case depending on the temperature and specimen orientation. These stress levels are considerably higher compared to the near equiatomic Ni compositions of these class of alloys. On the other hand, the maximum transformation strains, measured from incremental straining experiments in compression, were lower compared to both the phenomenological theory with Type II twinning and the previous experimental work on 50.8%Ni NiTi crystals. A new theory for compound twinning is introduced with lattice invariant shear as a solution, and relies on the successive austenite phase (B2) to intermediate phase (R) to martensite phase (B 19′) transformation. The compound twinning model predicts lower transformation strains compared to the Type II twinning case lending an explanation of the experimental transformation strain levels. 

*Keywords:* Shape memory; Martensite; Single crystal; Transmission electron microscopy (TEM); Phase transformations

## 1. INTRODUCTION

Phase transformations in nickel titanium alloys have been studied extensively with most emphasis placed on near equiatomic Ni–Ti compositions [1]. Two types of material response have been examined, namely “shape memory” and “pseudoelasticity”. The “shape memory” refers to the transformation of the material from martensite to austenite upon heating to a temperature exceeding the austenite start temperature. “Pseudoelasticity” is the forward transformation upon loading and reverse transformation upon unloading at temperatures above the austenite finish temperature. The pseudoleasticity temperature interval is approximately 80 K in equiatomic NiTi alloys. This temperature range is curtailed by the lack of slip resistance near the $M_d$ temperature. The $M_d$ temperature is defined as the highest temperature where pseudoleasticity can be observed. Majority of the work on NiTi alloys has considered aged conditions because the aging treatments produce pseudoleasticity near room temperature [1–3] and also raise the $M_d$ temperature. It has also been known that increasing the austenite strength increases slip resistance thereby extending the utility of these alloys to a wider temperature range. The strengthening of the austenite is achieved via deformation processing routes or with the fine precipitate structure. Nickel rich compositions (with at. Ni exceeding 51%) of NiTi alloys can be used to strengthen the austenite domains via high volume fraction of precipitates. Despite their strong potential, nickel rich NiTi alloys have been considered in only few studies [4]. The only notable

† To whom all correspondence should be addressed.
*E-mail address:* huseyin@uiuc.edu (H. Sehitoglu)

1359-6454/01/$20.00 
PII: S1359-6454(01)00216-6

work has been undertaken by Miyazaki and colleagues [4] who studied polycrystalline 51.6% Ni at. NiTi alloys. They noted that the 51.6% at. Ni NiTi alloy exhibits a lower martensite start temperature and higher slip resistance compared to its lower Ni counterparts. Further work is needed in Ni rich NiTi alloys to examine the possibility of a wider pseudoleasticity temperature interval and also high strength in both the austenitic and martensitic phases.

Upon austenite to martensite transformation in NiTi alloys the martensite is composed of internal twins in the B19′ phase, i.e., a twin related Correspondence Variant Pair (CVP) forms [2]. This martensite variant can be produced either by a single step of B2→B19′ transformation [5, 6], or by the successive B2→R-Phase→B19′ transformation [7–9]. Type II twinning has been dominantly observed in experiments and is confirmed to be lattice invariant shear. For the case of aged alloys "compound twinning" has also been identified experimentally [10–12] but ruled out as a lattice invariant shear based on theoretical considerations [13]. In other words, a theoretical solution for the twin and habit planes could not be obtained. An original calculation is presented in this paper addressing the successive B2 to R to B19′ transformation that produces "compound twinning" as a lattice invariant shear solution. The transformation strains associated with the compound twinning are shown to be lower compared to the Type II twinning solutions lending an explanation to the experimentally observed transformation strains levels.

Our previous work [2, 3] focussed on 50.8% at. Ni single crystals, and in this work the emphasis is placed on the 51.5% at. Ni NiTi composition. Also, in previous work we considered only aged materials, in the current work [2] we study both aged and solutionized materials. Higher strength levels for both the B2 (austenite) and the B19′ (martensite) phases are expected in this alloy. We demonstrate that the behavior of this class of alloys is similar to the 50.8% at. Ni case but with greater potential in actuator applications where ultra high strength in compression is desired. On the other hand, the transformation strains in the case of 51.5% at. Ni alloys (both in the solutionized and the overaged cases) are lower compared to the 50.8% at. Ni NiTi alloys (in compression). Possible reasons for this difference are rationalized based on a new theory for austenite to martensite transformation discussed above which admits the R-phase as an intermediate structure [5–9].

We note that in previous treatments the deformation experiments were conducted on polycrystals [1]. In the present work, five different crystallographic orientations ([001], [110], [111], [122] and [012] in the austenite crystal frame) were studied experimentally. These orientations were chosen because [001] and [012] represent the most favorable orientations for transformation in compression while the [111] and [122] represent the most difficult orientations for transformation in compression. Furthermore, the [001] case is of special interest because plastic deformation in this orientation is curtailed due to the operating {001}<001> and {011}<001> slip systems. TEM photographs of deformed [001] specimens confirm the lack of slip activity in this case. These results clearly show that the [001] crystal orientation exhibits an increase in flow stress with increasing temperature beyond the traditional pseudoelasticity regime for both the solutionized and overaged materials. Since the experiments were conducted at multiple temperature levels, it was possible to determine precisely the temperature range over which pseudoelastic response occurred. For the solutionized case, the $M_s$ temperature is below 77 K and pseudoelasticity has been observed in the experiments in the range 77–283 K. For the case of aged alloys, the $M_s$ temperature is near 236 K and pseudoelasticity is observed in the range 273–440 K.

The tensile ductility of the 51.5% at. Ni alloys is decreased compared to 50.8% Ni alloys. Because the present experiments were conducted under compression, fracture of the specimens did not occur. This is an important advantage of utilizing compression specimens. Consequently, the experiments have been carried out to strains of 9% or higher without difficulties, allowing examination of the plastic deformation behavior of austenite and martensite phases.

## 2. EXPERIMENTAL PROCEDURE

Single crystal Ti–51.5%Ni samples were prepared from a single material batch. The samples were grown by the Bridgman technique in an inert gas atmosphere. The orientation of single crystal specimens was determined by using Laue back-scatter diffraction patterns. Solutionizing of the specimens was conducted at 1273 K for 2 h in an inert gas atmosphere. Then, one set of specimens was examined in the solutionized state while the other set of specimens was aged at 823 K for 1.5 h. A Perkins–Elmer differential scanning calorimeter (DSC) was used to determine the transformation temperatures for the overaged case. The DSC results are shown in Fig. 1(a). The austenite start temperature, $A_s$, for overaged samples is 284 K while the $M_s$, martensite start temperature, is approximately 236 K. Other transformation temperatures are $A_f = 300$ K and $M_f = 223$ K. An intermediate phase, called the R-phase, appears in the DSC results which transforms to martensite upon further cooling. For the solutionized case, the transformation temperatures were too low (<77 K) to be detected by the DSC technique.

We note that the overaged microstructure is shown in Fig. 1(b) and (c). The approximate size of the $Ti_3Ni_4$ precipitates is 750 nm and the volume fraction is nearly 20%. Four variants of the $Ti_3Ni_4$ precipitates are present but fewer than four are visible on the microphotographs due to the specimen orientation [10]. The precipitates have a lens-like shape with their normal parallel to the $[111]_{B2}$ orientation of the

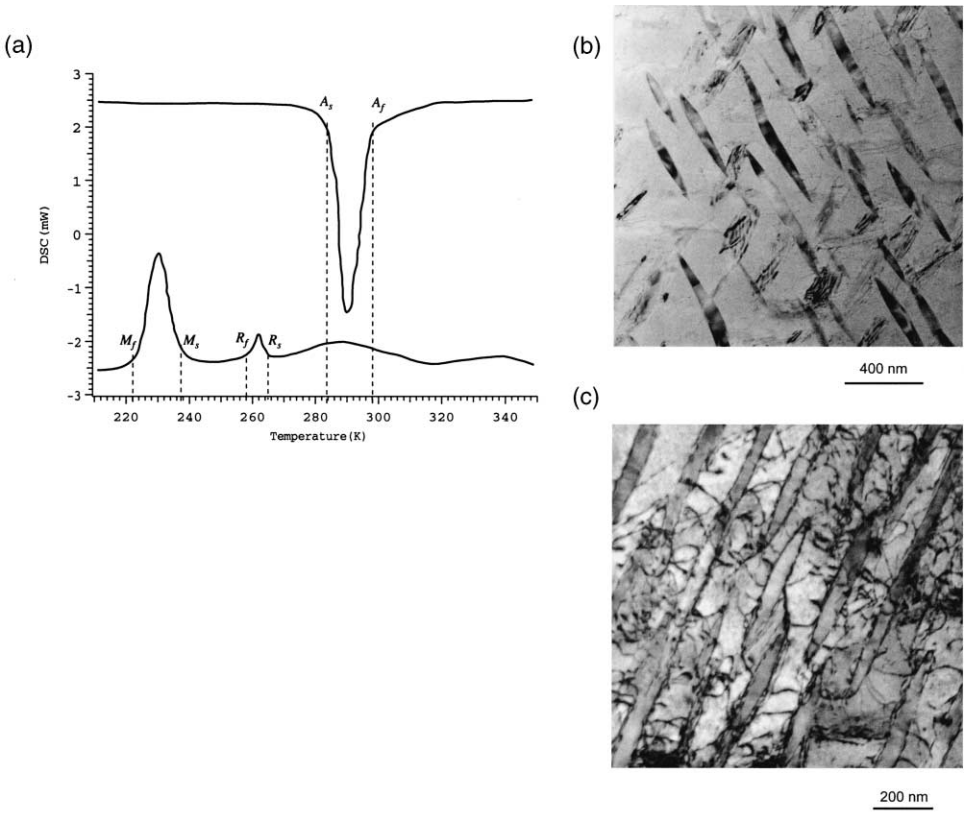


Fig. 1. (a) The differential scanning calorimetry results for the 51.5%Ni–NiTi alloy (overaged 823 K 1.5 h case). (b) The four variant precipitate structure in 51.5%Ni–Ti (only three variants are visible in this case) showing the undeformed structure. (c) The dislocation structure between the precipitates for the [111] overaged case after incremental straining deformation.

matrix. In Fig. 1(b) the precipitate structure is shown for the undeformed state of the material. We note that the precipitates do not transform to martensite. A significant decrease in the amount of material that can undergo transformation means that the experimental transformation strains would be lower than the theoretical values. In Fig. 1(c) the microphotograph of the [111] specimen is shown which has been deformed under incremental straining conditions. As discussed later, this orientation is favorable for slip deformation with presence of dislocations along the austenite channels (Fig. 1(c)).

The specimen has a square crossection with 4 mm width and 8 mm height. In the experiments, the loads were measured with a load cell, and strains were measured with a miniature MTS (Materials Test Systems) extensometer with a 3 mm gage length. The use of the miniature extensometer circumvents the end effects associated with stroke measurements. The strain rates were maintained at $10^{-4}$ l/s to minimize both the rate effects and temperature rise during the experiments.

The critical stress for transformation as a function of temperature has been determined with a series of deformation experiments. The results are summarized in Figs 2 and 3 for solutionized and overaged cases respectively. Companion samples were used to establish these points to avoid previous deformation effects on the results. The $M_s$ is obtained by extrapolation of the stress–temperature relation to zero stress as 230 K (average of all orientations) for the overaged case. This is consistent with the $M_s$ value obtained from DSC measurements. Such a comparison is not meaningful in the solutionized case and the behavior is rather complex.

At low temperatures, the strength of the solutionized case is rather high for orientations (especially [111] that do not favor the transformation). The [001] orientation for both the aged and solutionized cases exhibits similar stress–temperature behavior except that the $M_s$ temperatures are drastically different (near 230 K for aged and $<77$ K for the solutionized cases respectively). The slope of the stress–temperature relation in the pseudoleasticity regime is linear and this region is described with the Clausius–Clapeyron relation. The slope of the Clausius–Clapeyron curve ($A \rightarrow M$ region) is on the average 6.5 MPa/°C. The $M_d$ temperature is defined here as the maximum temperature (nearly 360 K for the overaged case) below which pseudoleastic deformation occurs. Note that the $M_d$ temperature depends on the crystal orientation but it cannot be identified for the [001] case because slip is curtailed in this

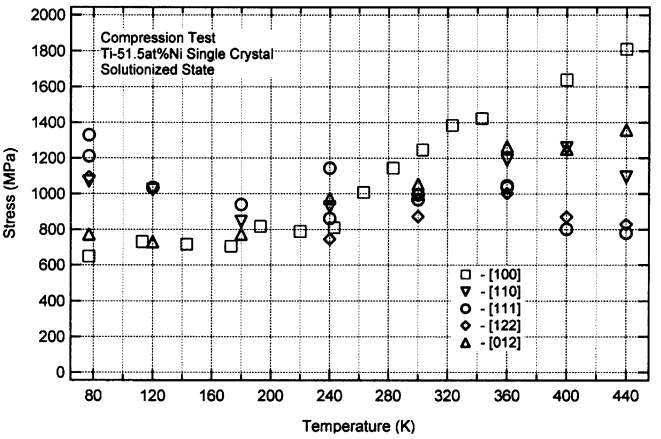


Fig. 2. Transformation stress (0.2% offset) as a function of temperature under compression; solutionized case.

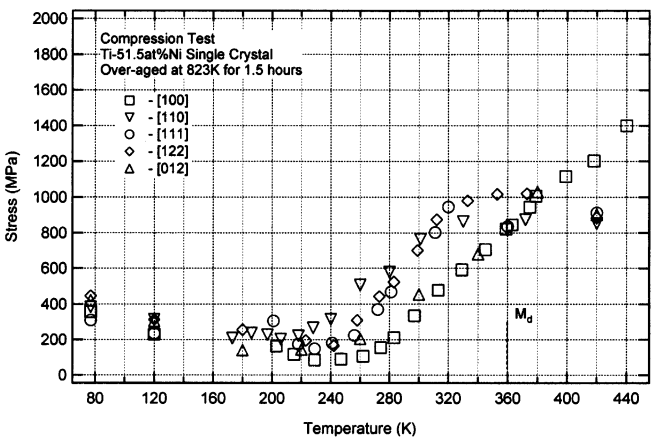


Fig. 3. Transformation stress (0.2% offset) as a function of temperature under compression; overaged case.

orientation. Also, for the case of solutionized samples, the $M_d$ cannot be clearly established for any of the crystal orientations.

The most significant finding in these experiments is the following. In the [001] orientation the critical stress for transformation continues to increase with temperatures well past 400 K for both the overaged and the solutionized cases. TEM photographs (to be shown later) indeed confirm the lack of slip in this orientation.

## 3. CALCULATION OF THEORETICAL TRANSFORMATION STRAINS

Upon austenite to martensite transformation in NiTi alloys (either due to stressing above $M_s$, or cooling below $M_s$) the martensite is composed of internal twins in the B19′ phase, i.e., a twin related Correspondence Variant Pair (CVP) forms [2]. This martensite variant can be produced either by a single step of B2→B19′ transformation [5–7], or by the successive B2→R-Phase→B19′ transformation [7–9]. There are 12 lattice correspondence variants for B2→B19′ transformation [6] and 8 twinning types can be formed within these 12 lattice correspondence variants [2, 14]. Based on crystallography, some twinned variant pairs are able to form the so called "habit plane" variants since their deformations are compatible with B2 phase or R-Phase. Type II twinning has been dominantly observed in experiments and is confirmed to be lattice invariant shear. In Type II twinning the twin plane normal is irrational. For the case of aged alloys compound twinning has also been identified experimentally [9–12] but ruled out as a lattice invariant shear based on theoretical considerations [13].

In the present work, regardless of the twin type, each martensite CVP is described by a unique habit plane normal, $\boldsymbol{m}$, and transformation direction, $\boldsymbol{b}$. Two cases are considered in this work: (i) the Type II twinning solution, and (ii) the two step transformations of B2→R-Phase→B19′ transformation resulting in compound twinning. We now summarize the methods for determination of the habit plane para-

meters and the transformation strains associated with each solution.

### *3.1. Type II twinning*

In the parent phase coordinate system (B2), the deformation matrices of the 12 B19′ lattice correspondence variants are designated as $\boldsymbol{U_1}$, $\boldsymbol{U_2}$,…,$\boldsymbol{U_{12}}$. For a given variant pair (***Ui***, ***Uj***), the twin plane ***n*** and twin shear ***a*** can be determined by using the condition that the interface between the two lattice correspondence variants in the twin is an invariant plane (unrotated and undistorted) [14, 15]

$$\boldsymbol{R}_{ij}\boldsymbol{U}_j - U_i = \boldsymbol{a} \otimes \boldsymbol{n} \tag{1}$$

where ***Rij*** is an orthogonal tensor (of rank 2) satisfying $\boldsymbol{R}_{ij}^T\boldsymbol{R}_{ij} = \boldsymbol{I}$ (***I*** is second rank identity tensor, and the superscript *T* represents the transpose of a matrix). The ⊗ represents a dyadic product. The tensor ***Rij*** represents the relative rotation between the two variants. The twinned martensite is composed of correspondence variant pairs with a certain volume ratio. When there are finite number of twin layers, the deformation of martensite is represented as

$$\boldsymbol{F}_{\mathbf{M}} = \boldsymbol{R}_h[f\boldsymbol{R}_{ij}\boldsymbol{U}_j + (1-f)\boldsymbol{U}_i] \tag{2}$$

where ***Ui*** and ***Uj*** are the two lattice correspondence variants in the twin, and $(1-f)$ and $f$ are respectively their volume fractions. The tensor ***Rh***, is the relative rotation between the twinned martensite and the parent phase. The habit plane ***m*** and transformation shear ***b*** can be obtained by

$$\boldsymbol{F}_{\mathbf{M}} - \boldsymbol{I} = \boldsymbol{b} \otimes \boldsymbol{m} \tag{3}$$

where ***I*** is the identity tensor representing the undeformed austenite, ***m*** is the habit plane normal and ***b*** is the shear of the martensite. In equations (1)–(3), the known parameters are ***Ui***, ***Uj***, and all the other unknowns can be solved from the equations. The lattice parameters of B2 phase and B19′ phases must be known [6]. For the B2 phase $a_0 = 3.015$ Å, and for the B19′ phase: $a = 2.889$ Å, $b = 4.120$ Å, $c = 4.622$ Å, $\theta = 96.8°$.

The base crystallographic parameters for solutionized NiTi produce two solutions as: ***m*** = 0.8889,0.4044,0.2152, ***b*** = <0.0568,0.0637,0.0991> and ***m*** = 0.3762,0.5136,0.7712, ***b*** = <0.1195,0.0485, 0.0216> [2]. The habit plane solutions above are obtained using {0.7205, 1, 0}<001> Type II-1 twinning (we use the term Type II-1 because there exists another {1, 1, 3.0495}<−1, 1, 0> Type II variants which are designated as Type II-2) which is consistent with the dominant mode experimentally observed. In Type II twinning the twin plane normal is irrational while in Type I the twin plane normal is rational. Once the habit plane normals and transformation shears are determined, it is possible to establish the transformation strain as,

$$\varepsilon = \frac{1}{2}(\boldsymbol{F}_{\mathbf{M}}^T\cdot\boldsymbol{F}_{\mathbf{M}} - I) \tag{4}$$
$$= \frac{1}{2}[\boldsymbol{b}\otimes\boldsymbol{m} + \boldsymbol{m}\otimes\boldsymbol{b} + (\boldsymbol{b}\cdot\boldsymbol{b})\boldsymbol{m}\otimes\boldsymbol{m}]$$

The last term in equation (4) represents finite strain effects. The transformation strain contours corresponding to equation (4) are provided in Fig. 4(a) for compression and Fig. 4(b) for tension. The small deformation theory (without the last term in equation (4)) produces recoverable strains in compression which are in approximately 10% higher than the large deformation theory (Green strain) used in equation (4). The transformation strain results for compression for the five orientations considered in this study are given in Table 1 as the third column. The resolved shear stress factor (RSSF) for Type II-1 twinning (compression) is included in Table 1 as second column. The first column in Table 1 lists all the orientations of interest in our study. The resolved shear stress factor, RSSF (for Type II-1 twinning), is simply defined as,

$$\text{RSSF} = (\boldsymbol{b}\cdot e)(\boldsymbol{m}\cdot e)/|\boldsymbol{b}| \tag{5}$$

where $e$ denotes the crystallographic direction of interest. Note that the RSSF can be larger than 0.5 because the transformation direction and the transformation plane are not necessarily orthogonal.

### *3.2. Compound twinning*

It has been generally accepted that [011] Type II and [111] Type I are the major twinning modes that produce lattice invariant shear in B2 to B19′ transformation. However, there is increasing evidence that [001] compound twinning mode has been observed repeatedly by several researchers [10–12]. In NiTi alloys there exists a so-called "premartensitic" rhombohedral phase (R-Phase) formed as a precursor to the B19′ martensitic transformation [7–9]. Based on the phenomenological theory of crystallographic transformation or the energy minimization theory [15], it is impossible for the compound twin to constitute a lattice invariant shear during the B2 to B19′ martensitic transformation. In view of the experimental evidence for the observation of compound twinning in B19′ martensite [10–12, 16, 17], in this work, we analyzed a compound twinned B19′ martensite during the R-Phase to B19′ transformation.

There are four lattice correspondence variants for the B2 to R-Phase transition and the corresponding deformations can be represented in the B2 coordinate system as [8, 9]

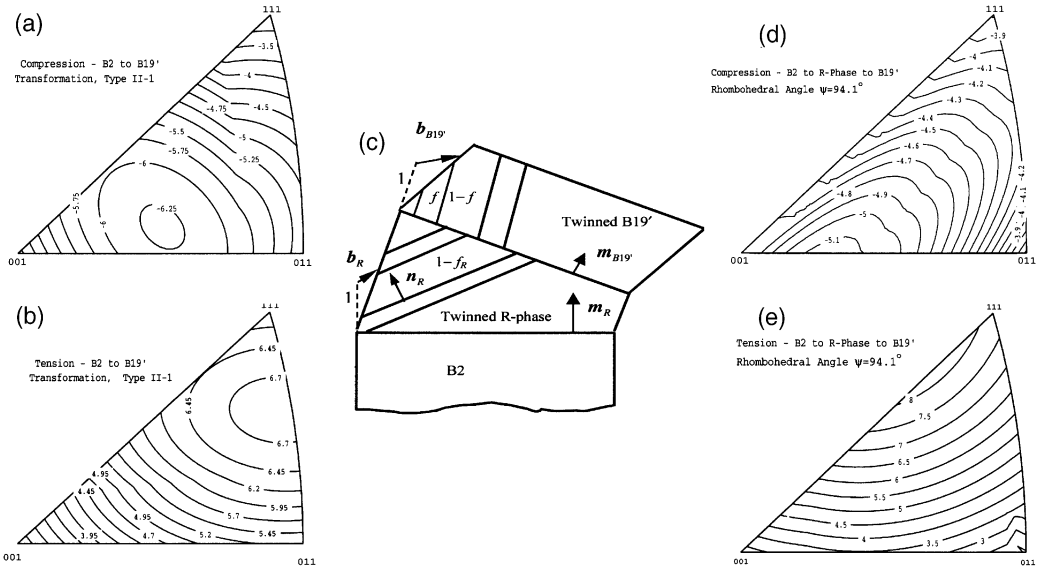


Fig. 4. (a) Transformation strain contours for Type II twinning case [2] (compression). (b) Transformation strain contours for Type II twinning case (tension). (c) A schematic of two stage transformation from the austenite to R-Phase to martensite. (d) The transformation strain contours for B2 to R-Phase to compound twinned B19′ (compression). (e) The transformation strain contours for B2 to R-Phase to compound twinned B19′ (tension).

Table 1. Theoretical RSSF (Resolved Shear Stress Factor) and the compressive transformation strains for the Type-II-1 twinning, compound twinning of B19′, and the deformed austenite Type-II-1 case for compression. The last two columns are the experimentally determined recoverable strains for the solutionized and the overaged cases respectively (compression)

| Crystallographic Direction | RSSF B2→B19′ -Type II-1 Twinning | Type II-1 Twinning-(%) | B2→R→B19′ Strain of Compound Twinned B19′ (%) | Experimental Recoverable Strains (%) | |
|---|---|---|---|---|---|
| | | | | Solutionized | Overaged |
| [001] | 0.386 | 4.38 | 4.73 | 3.9 | 3.3 |
| [110] | 0.430 | 5.06 | 3.57 | 4.2 | 3.7 |
| [111] | 0.253 | 2.98 | 3.79 | 1.2[a] | 3.0 |
| [012] | 0.508 | 6.23 | 4.99 | 3.7 | 3.2 |
| [122] | 0.370 | 4.54 | 4.24 | 0.76[a] | 2.3 |

[a] plastic deformation dominates the stress-strain response.

$$U_1 = \begin{bmatrix} \alpha & \beta & \beta \\ \beta & \alpha & \beta \\ \beta & \beta & \alpha \end{bmatrix}, U_2 = \begin{bmatrix} \alpha & -\beta & \beta \\ -\beta & \alpha & -\beta \\ \beta & -\beta & \alpha \end{bmatrix}, \quad (6)$$

$$U_3 = \begin{bmatrix} \alpha & \beta & -\beta \\ \beta & \alpha & -\beta \\ -\beta & -\beta & \alpha \end{bmatrix}, U_4 = \begin{bmatrix} \alpha & -\beta & -\beta \\ -\beta & \alpha & \beta \\ -\beta & \beta & \alpha \end{bmatrix} \quad (7)$$

where $\alpha = (\sqrt{1 + 2\cos\psi} + 2\sqrt{1-\cos\psi})/3$, $\beta = (\sqrt{1 + 2\cos\psi} - \sqrt{1-\cos\psi})/3$ and $\psi$ is the rhombohedral angle. The B2 phase and rhombohedral phase have the same unit cell length of $a_0 = 3.015$ Å.

Similar to the B2 to B19′ transformation, B2 to R-Phase transformation is controlled by

$$\boldsymbol{T_{AB}U_B} - \boldsymbol{U_A} = \boldsymbol{a_R} \otimes \boldsymbol{n_R} \quad (8)$$

$$\boldsymbol{F_R} = \boldsymbol{T}_h[f_R \boldsymbol{T_{AB}U_B} + (1-f_R)\boldsymbol{U_A}] \quad (9)$$

$$F_R - I = \boldsymbol{b_R} \otimes \boldsymbol{m_R} \quad (10)$$

where $\boldsymbol{U_A}$, $\boldsymbol{U_B}$ are two variants within the 4 R-Phase variants, $\boldsymbol{T_{AB}}$ is the relative rotation between variants *A* and *B* in the twin, $(1-f_R)$ and $f_R$ are the volume fraction of variants *A* and *B*, respectively. The tensor $F_R$ represents the average deformation of twinned R-Phase, $\boldsymbol{I}$ is the deformation of austenite, $\boldsymbol{Th}$ is the relative rotation between R-Phase and austenite, and $\boldsymbol{a_R}$, $\boldsymbol{n_R}$, $\boldsymbol{b_R}$, $\boldsymbol{m_R}$ are respectively the twinning shear, twinning plane, transformation shear and habit plane of R-Phase. The relevant vectors are shown in the schematic given as Fig. 4(c). From these equations

we can see that the R-Phase is not a single lattice correspondence variant, but is twin related. This has also been confirmed with experimental observations [8, 9] Two solutions of {100}<011> and {110}<011> compound twins are obtained from equation (8) depending on the rhombohedral angle $\psi$. The volume fraction $f_R$, habit plane normal $\boldsymbol{m}_{\mathbf{R}}$ and transformation shear $\boldsymbol{b}_{\mathbf{R}}$ can be obtained from equations (9) and (10) for a given variant pair $\boldsymbol{U}_{\mathbf{A}}$ and $\boldsymbol{U}_{\mathbf{B}}$. There are 24 habit plane variants with {100}<011> compound twinning when $\psi>90°$, while no variants with {100}<011> compound twinning exist when $\psi<90°$. The transformation shears and habit plane normals for the {100}<011> compound twinning variants are $\psi$-dependent, as well as the volume fraction $f_R$. The habit plane variants with {110)<001> compound twins can be obtained in both cases of $\psi>90°$ and $\psi<90°$, and the number of variants is 12. The transformation shears and habit plane normals for these variants are $\psi$-dependent, while the volume fraction $f_R$(=0.5) is $\psi$-independent.

The R-Phase to B19′ martensitic transformation is controlled by

$$F_{B19'} - F_R = \boldsymbol{b}_{\mathbf{B19'}} \otimes \boldsymbol{m}_{\mathbf{B19'}} \tag{11}$$

where $m_{B19'}$ is the habit plane normal between R-Phase and B19′, $\boldsymbol{b}_{\mathbf{B19'}}$ is the transformation shear. The $F_{B19'}$ is the average deformation of B19′ martensite, which has the same form as $\boldsymbol{F}_{\mathbf{M}}$ in equation (2). Selecting a certain $\boldsymbol{F}_{\mathbf{R}}$ as matrix and substituting equations (1) and (2) into equation (11), $\boldsymbol{b}_{\mathbf{B19'}}$ and $\boldsymbol{m}_{\mathbf{B19'}}$ can be obtained. When $|\psi-90°|\leq 2.7°$, the results are similar with those of single step B2 to B19′ transformation, specifically, there are 48 habit plane variants with Type I-1, Type I-2, Type II-1 and Type II-2 twins [2]. When $|\psi-90°|>2.7°$, the numbers of habit plane variants for each twinning type are less than 48 and it is possible to obtain the habit plane variants with other type of twins. What we are most interested in is when $\psi$ is in the range between 93.9° and 95.1°. Then, the habit plane variants with compound twins are obtained. The solutions are given in Table 2 for $\psi = 94.1°$. We note that for the {001}<100> compound twinning case there are two twins with different volume fraction and each volume fraction gives two sets of solutions. The corresponding transformation strain contours for B2→R-Phase→B19′ transformation are shown in Fig. 4(d) for compression. Similar results for tension case are given in Fig. 4(e). The tensile results are included as a reference for comparison and point to higher transformation strains compared to compression. The transformation strain levels for orientations studied in the present work are listed in Table 1 for compression (fourth column). The results were calculated by using $\psi = 94.1°$. The highest transformation strain is determined by selecting the maximum RSSF from all possible solutions and calculating the accompanying transformation strain. The results show that the transformation strains of compound twinned martensite are smaller compared to the case of Type II-1 twinning (compare Fig. 4(a) and (d) with Fig. 4(b) and (e)).

Table 2. The theoretical results for the habit plane normal, transformation direction and the volume fraction of twins for the compound twinned B19′ martensite during R to B19′ transformation

| Solutions of {011}<100> compound twinned B19′ martensite |
|---|
| $f = 0.18278$, $\lvert\boldsymbol{b}_{\mathbf{B19'}}\rvert = 0.1406$ |
| $\boldsymbol{m}_{\mathbf{B19'}} = (-0.4080, 0.8756, -0.2585)$, $\boldsymbol{b}_{\mathbf{B19'}} = [0.1043, 0.0273, -0.0903]$ |
| $\boldsymbol{m}_{\mathbf{B19'}} = (-0.7096, -0.2546, 0.6569)$, $\boldsymbol{b}_{\mathbf{B19'}} = [0.0647, 0.1212, 0.0300]$ |
| $f = 0.57518$, $\lvert b_{B19'}\rvert = 0.1436$ |
| $\boldsymbol{m}_{\mathbf{B19'}} = (-0.3896, -0.3047, 0.8691)$, $\boldsymbol{b}_{\mathbf{B19'}} = [0.1090, -0.0907, 0.0225]$ |
| $\boldsymbol{m}_{\mathbf{B19'}} = (-0.7277, 0.6503, -0.2178)$, $\boldsymbol{b}_{\mathbf{B19'}} = [0.0637, 0.0373, 0.1232]$ |

## 4. EXPERIMENTALLY DETERMINED STRESS–STRAIN RESPONSE IN THE TEMPERATURE RANGE 77–440 K

The stress–strain response of 51.5Ni–Ti (at small strains) over a broad range of temperatures are summarized in Fig. 5(a) and (b). In these experiments the specimens were strained to 3% in compression and unloaded to zero stress. The [001] orientation is chosen to illustrate the stress–strain results in Fig. 5(a) and (b) for solutionized and aged cases respectively. For the solutionized case, the pseudoleastic response is observed at temperatures as low as 77 K and extends to temperatures near 300 K. These results point to the enormous capability of 51.5%Ni alloys to exhibit transformation over a broad range of temperatures. Some degree of shape memory was observed at 77 K and at higher temperatures but 80% of the transformation strains was comprised of pseudoleastic strains. The range of pseudoleastic response is indicated on the figure. As the temperatures exceed 300 K the deformation could not be recovered. When the material is overaged the martensite start temperature increases to 236 K and the stress-induced transformation occurs over the range 270–440 K. These results are illustrated in Fig. 5(b). The strength levels observed in this case are lower than the solutionized case, and nearly 100% pseudoleasticity is observed at temperatures above 270 K. Similarly, the range of pseudoleasticity temperature interval is marked on the figure.

To gain insight into the recoverable strains under the application of larger strains, and to establish the maximum recoverable strains, a series of incremental straining experiments have been conducted. In these experiments, the strain is progressively increased in increments of 2%, and upon unloading the specimen was heated to 373 K to realize the shape memory strains. The results of the incremental straining experiments for the solutionized case are given in Fig. 6(a)–(e) at 77 K. These experiments were conducted on all five orientations considered in this study. The transformation (recoverable) strains were a summation of pseudoleastic and shape memory strains

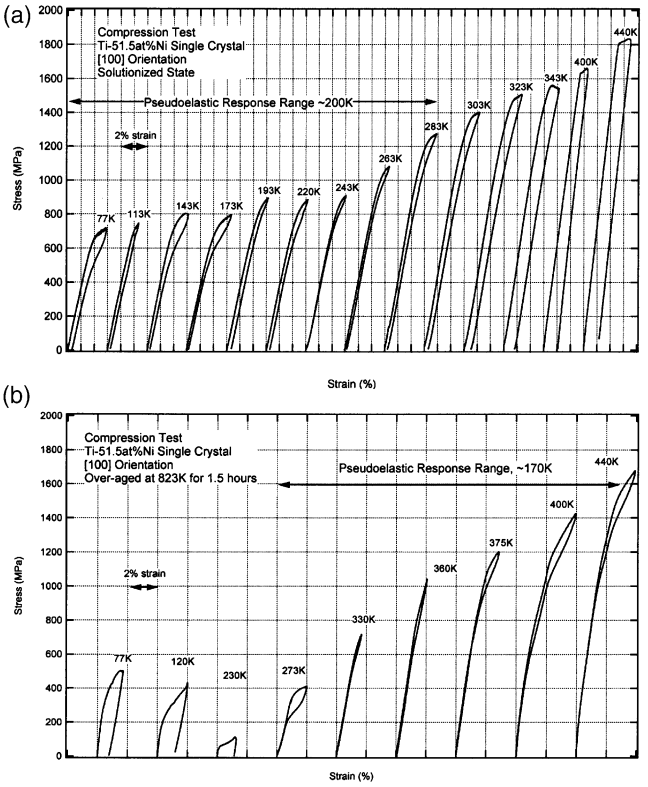


Fig. 5. (a) The compressive stress–strain response of 51.5%-Ni [001] solutionized case as a function of temperature; (b) overaged case.

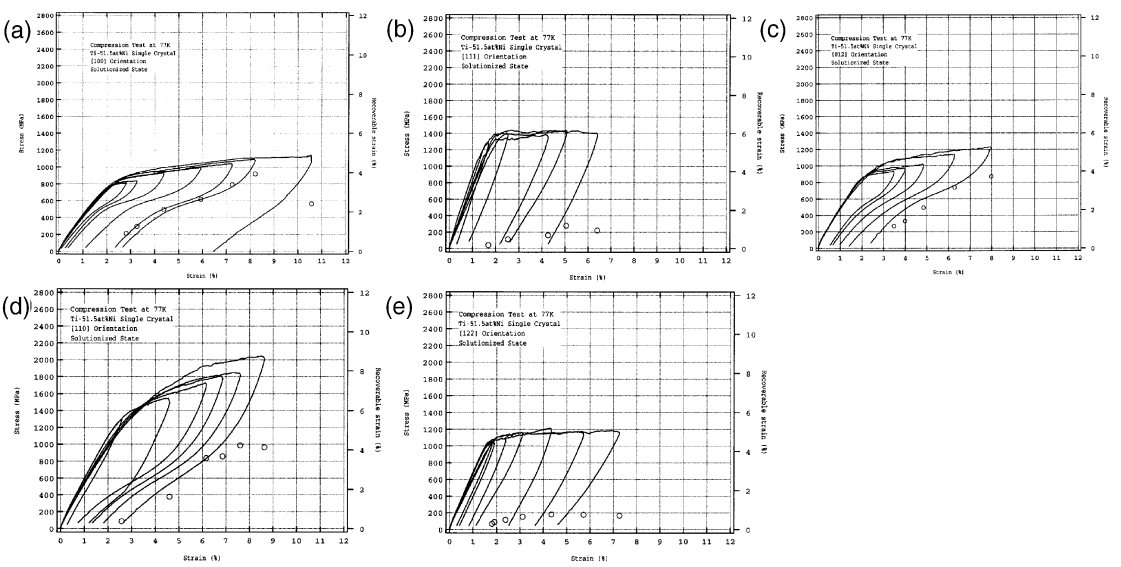


Fig. 6. Stress–strain response and the evolution of transformation strains at 77 K (a) for the [001] solutionized case, (b) for the [110] solutionized case, (c) for the [111] solutionized case, (d) for the [122] solutionized case and (e) for the [012] solutionized case.

where the shape memory component was rather small. This is in contrast to the behavior of <51% Ni NiTi alloys where at low temperatures shape memory behavior dominates while at higher temperatures pseudoleastic response is most prevalent. Experiments were conducted at 77 K because at this temperature the transformation strains are higher compared to higher temperatures. This was confirmed with experiments at higher temperatures. The recoverable strain levels are shown with data points in Fig. 6(a)–(e) and they increase with increasing strain, reach a maximum and then decrease with further

straining. The maximum recoverable strains are listed in Table 1 and are in the range 0.76% to 4.2%. We note that in the [111] and [122] orientations the material undergoes predominantly plastic deformation (see Fig. 1(c) for a TEM microphotograph) and the amount of recoverable strains is rather small.

The results of the incremental straining experiments at room temperature for the overaged case are given in Fig. 7(a)–(e). We note that the room temperature coincides with the austenite finish temperature, therefore, pseudoleastic response dominates at low strains. At higher strain levels the transformation could not be fully recovered upon unloading, and heating to 100°C was required for further recovery. The [001] orientation [Fig. 7(a)] exhibits elastic response after austenite–martensite transformation because plastic deformation due to slip is curtailed in the austenitic domains. The recoverable transformation strains are comparable to the solutionized case; we note, however, that the [111] and [122] orientations display significantly higher recoverable strains (3.0% and 2.3% respectively) compared to the solutionized case. The results of the experimental recoverable strains are listed in Table 1 (6th col.). Overall,

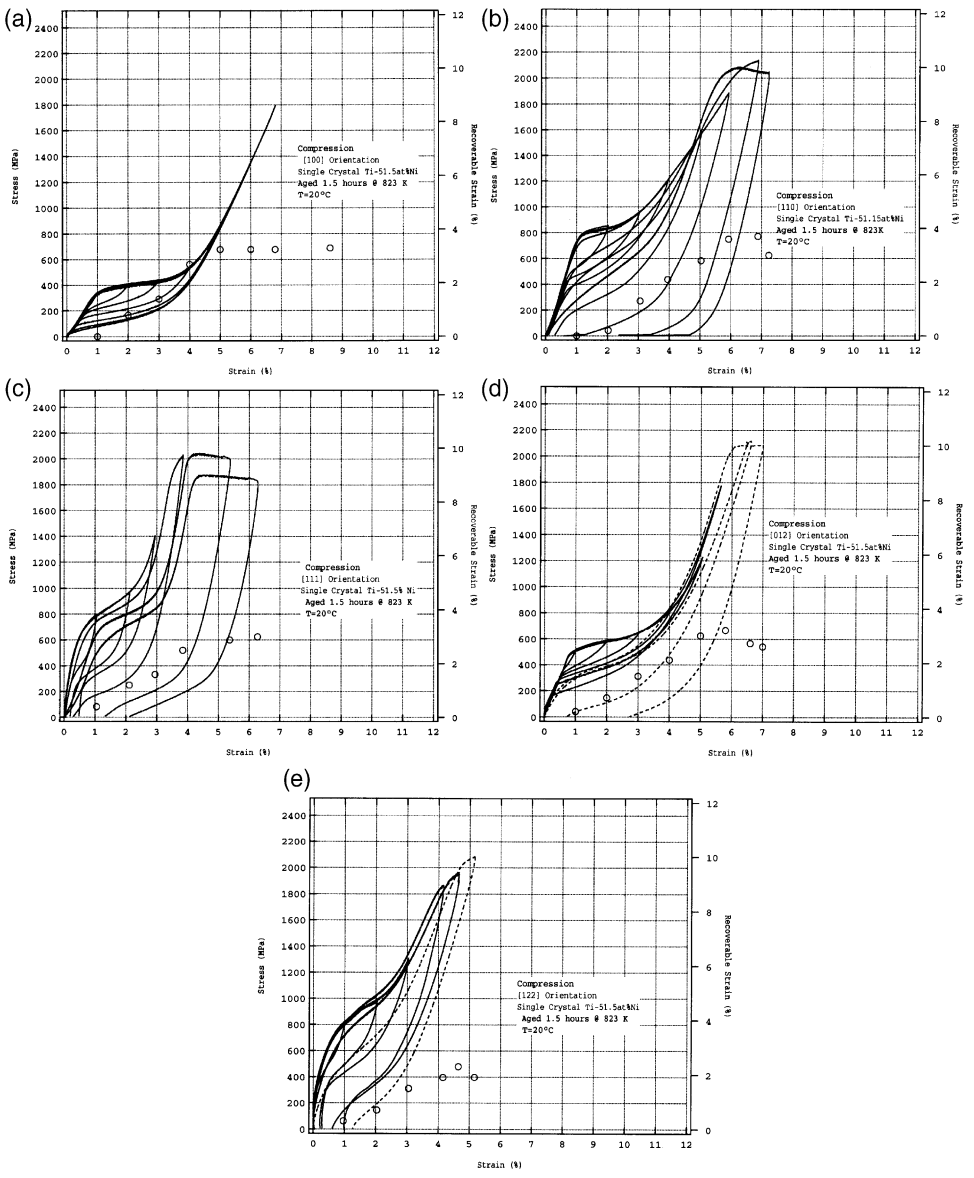


Fig. 7. Stress–strain response and the evolution of transformation strains at 293 K (a) for the [001] overaged case, (b) for the [110] overaged case, (c) for the [111] overaged case, (d) for the [012] overaged case and (e) for the [122] overaged case

the stress levels of the 51.5%Ni alloys are 800 MPa compared to 400 MPa values for the 50.8% Ni alloy studied previously [2].

## 5. DISCUSSION OF RESULTS

The results for the 51.5%Ni–Ti alloys show for the first time that the temperature range over which pseudoleasticity develops is as high as 200 K for the case of [001] orientation [see Fig. 5(a) and (b)]. This extends the utility of the NiTi alloys over a temperature range at least two times higher than the previously reported range of 80 K [1, 18, 19]. If we can tailor the texture of polycrystals to a [001] type then we can develop superior compressive actuators. In the case of [012] orientation, the temperature range of stress-induced transformation exceeds 100 K, while for the [111] case transformation does not occur due to slip deformation at all temperatures studied here. One major difference between the 51.5%Ni and the 50.8%Ni alloys is that the strength levels in 51.5%Ni are higher by as much as 400 MPa over the entire stress-induced transformation regime [2]. This makes 51.5%Ni attractive in specific applications where high strength shape memory alloys are required with large recoverable forces.

The experimental results demonstrate that the recoverable (transformation) strains for the 51.5%Ni composition are lower than the 50.8%Ni alloys [2]. One possible explanation for the lower transformation strains for the higher nickel material is the higher volume fraction of precipitates (20%) which are untransformable. The second reason, which is explored in this study, is that the transformation occurs through a two step B2 to R to B19′ transformation with compound twinning. The compound twinning produces a lower transformation strain compared to the Type II twinning case (Fig. 4(a),(b),(d) and (e)).

The [001] orientation has a Schmid factor for slip of zero for the {001}<001>and {011}<001> systems [20]. Therefore, slip cannot operate in this orientation. To illustrate this point the TEM results obtained from the 440 K straining case are presented in Fig. 8(a) and (b). Unlike other orientations [Fig. 1(c)], there is no indication of slip activity in the [001] case. Both TEM microphotographs are obtained from the same location with Fig. 8(b) displaying the precipitate and austenite domains at a higher magnification. Twinning at high temperatures has been observed in the [001] orientation as a main mechanism of plastic deformation [20]. The pseudoleasticity temperature interval is observed for the <001> case as 200 K, which far exceeds the levels in <111>, <122> and <112> orientations.

Due to the presence of the precipitates, there are multiple nucleation sites for martensite formation, and multiple variant formation. The number of variants activated is expected to differ from the phenomenological theory. The resultant multi-variant structure produces transformation strains that exhibit smaller orientation dependence compared to the previous work on 50.8% Ni crystals. For example, for the 51.5% Ni alloy, the transformation strains are in the range 2.3–3.7% for the overaged case (Table 1). The variation in the transformation strains for the 50.8% material was in the range 2.5–5.6% [2]. We also note the absence of the plateau regions in the stress–strain curves (Fig. 6(a),(b) and (e) and Fig. 7(a)–(e)), which are characteristic of the transform-

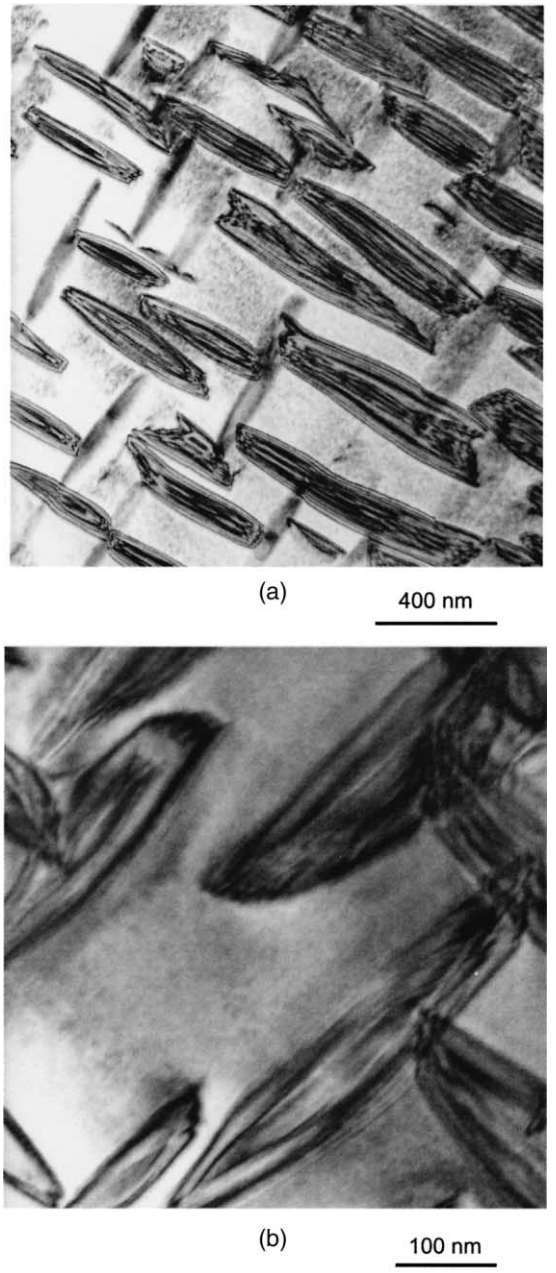


Fig. 8. (a) The precipitate structure and the surrounding matrix for the [001] compression experiment under straining at 440K. (b) The same location as (a) but a higher magnification demonstrating that slip activity is indeed absent for this orientation.

ation boundary motion of a single variant. The presence of the precipitates also influences the back stress, which governs the reverse transformation stress and the overall hysteresis stress range. With increasing strain in Fig. 7(a)–(e), the reverse transformation stress level decreases. Ultimately, the reverse transformation stress nears zero stress for favorable orientations upon unloading from large strains.

For the NiTi alloys, it has been widely recognized that <011> Type II twinning is the most prevalent twinning mechanism in B19′ martensites. There are, however, a number of investigations [11, 12, 17] where (001) compound twinning has been reported. Because the (001) compound twinning is not a lattice invariant shear, it has been viewed as deformation twinning by a number of investigators. We demonstrated in this study that compound twinning is indeed a lattice invariant shear if the transformation to B19′ is achieved via a two step B2 to R to B19′ transformation. The first study that analyzed such a two step transformation (B2 to R to B19′) was reported by Krishnan[ [12]. However, we note that the compound twinning solution presented in this paper is different from Krishnan's in several respects. We provide a solution for major and minor twin volume fractions within the B19′ phase and is not restricted to the $f = 0.5$ assumption made by Krishnan [12]. Also, we treat the R-phase as internally twinned as opposed to the single crystal R phase assumed by Krishnan [12]. The results confirm that the transformation strains for the compound twinning case [Fig. 4(a),(b),(d) and (e)] are lower than the Type II-1 twinning results.

Our previous work has shown that the end of the stress plateau is not the end of the stress-induced transformation [2]. During austenite to martensite transformation large regions of undeformed austenite exists which undergoes slip deformation [2]. If the slip deformation in the austenite regions is curtailed via crystal orientation or different processing routes, this would increase the recoverable strains considerably. The calculations for the Schmid factors of the austenite (Table 3) pointed out the lowest Schmid factors near the [001] pole resulting in transformation (Fig. 7(a)) under elastic conditions. Austenite yielding is not expected in this orientation due to the prevailing {001}<001> and {011}<001> slip systems [2, 20]. The critical stress versus temperature results given in Figs 2 and 3 confirm the remarkable resistance to slip in the [001] direction. In particular, in both the solutionized and overaged cases, the increase in flow stress with increasing temperatures in excess of 400 K is remarkable.

We note that the critical stress for martensite yielding is rather high and is of the order of 2000 MPa while the austenite yield levels are of the order of 1200 MPa. The austenite yield stress at room temperature can be established by extrapolating the critical stress versus temperature slope (beyond $M_d$) to lower temperatures. This is easier to demonstrate for the case of overaged material (Fig. 3). Ultimately, when martensite yielding occurs then the recoverable strains decrease with further increase in applied strain (see Fig. 6(a) and Fig. 7(b),(d) and (e) for a clear display). Therefore, any treatments that increase the critical austenite stress, such as through increase in volume fraction of precipitates, or texture in the case of polycrystals would increase the transformation strain.

Another important observation is that the $M_d$ temperature is nearly 360 K for the overaged crystals in all the crystallographic orientations except the [001] case where the $M_d$ temperature is much higher. Since the $M_s$ temperature has been measured as 236 K for the overaged case the range of transformation is at least 120 K for most orientations while this range is in excess of 200 K in [001] orientation. Also, the strength increases with increasing temperature in the range 200–360 K for the solutionized case for all crystal orientations. In the [001] case the increase in strength occurs well past 360 K. The results show that the deformation temperature relative to the $M_d$ temperature is an important consideration in interpretation of the stress–strain response.

Table 3. Calculated Schmid factors for the austenite slip systems

| Crystal orientation | Schmid factor—austenite {001}<001> | Schmid factor—austenite {011}<001> |
|---|---|---|
| [001] | 0.00 | 0.00 |
| [110] | 0.50 | 0.50 |
| [111] | 0.33 | 0.47 |
| [012] | 0.40 | 0.28 |
| [122] | 0.33 | 0.47 |

## 6. CONCLUSIONS

1. The strength of the 51.5Ni–Ti alloys is substantially higher (nearly 400 MPa) than the 50.8%Ni NiTi alloys both in the martensitic and the austenitic states. The strength of the [001] orientation increases with increasing temperature exhibiting pseudoleasticity over a broad range of temperatures. This orientation does not display an $M_d$ temperature up to 440 K. In other orientations the pseudoleasticity is substantially lower compared to the [001] case. The results confirm that [001] orientation can be exploited for specific applications.
2. The strength of the solutionized alloy is substantially higher than the overaged case at low temperatures. The solutionized condition exhibits higher transformation strains compared to the overaged case in [001] and [011] (~3.9 and 4.2% respectively) but much lower transformation strains in [111] and [122] orientations (<1%). Slip deformation is forwarded as an explanation for the

very low transformation strains in the [111] and [122] directions.

3. The overaged specimens exhibit pseudoleasticity and shape memory at temperatures above 273 K. The experimental transformation strain levels are substantially lower than the theoretical calculations in compression. Two factors were suggested to explain the lower transformation strains observed. These include the inability of the precipitates to transform and the compound twinning solution producing lower transformation strains.
4. A new model for transformation was introduced with compound twinning as a lattice invariant shear solution. A solutions was obtained for the two stage B2→R→B19′ transformation. In the development of this model, the R-phase is internally twinned and no assumptions were made regarding the twin volume fractions in the B19′ phase. The results point out that depending on the crystal orientation and the loading direction, the two stage transformation produces compound twinning with lower transformation strains compared to the Type II-1 twinning (single step transformation) in compression.

*Acknowledgements*—Portions of the research is supported by a grant from the National Science Foundation contract CMS 99-00090, Mechanics and Materials Program, Arlington, Virginia, and Air Force Office of Scientific Research, Directorate of Aerospace and Materials Sciences, Arlington, Virginia. Professor Chumlyakov received support from the Russian Fund for Basic Researches, Grant Nos. 02-95-00350, 99-03-32579. The facilities at Microanalysis of Materials, Materials Research Laboratory were used. This laboratory is funded by DOE-DMS grant DEFGO2-96ER45439.

## REFERENCES

1. Funakubo, H., *Shape Memory Alloys*. Gordon and Breack Science Publishers, New York, 1987.
2. Sehitoglu, H., Karaman, I., Anderson, R., Zhang, X., Gall, K., Maier, H. J. and Chumlyakov, Y., *Acta mater.*, 2000, **48**(13), 3311.
3. Gall, K., Sehitoglu, H., Chumlyakov, Y. and Kireeva, I., *Acta mater.*, 1999, **47**(4), 1203.
4. Miyazaki, S., Igo, S. and Otsuka, K., *Acta mater.*, 1986, **34**, 2045.
5. Otsuka, K., Sawamura, T. and Shimizu, K., *Phys. Stat. Sol.*, 1971, **5**(a), 457.
6. Matsumoto, O., Miyasaki, M., Otsuka, K. and Tamura, H., *Acta mater.*, 1987, **35**, 2137.
7. Ling, H. C. and Kaplow, K., *Metall Trans.*, 1980, **11A**, 77.
8. Miyazaki, S. and Wayman, C. M., *Acta metall.*, 1988, **36**(1), 181.
9. Miyazaki, S., Kimura, S. and Otsuka, K., *Phil. Mag. A*, 1988, **57**(3), 467.
10. Nishida, M., Wayman, C. M. and Chiba, A., *Metallography*, 1988, **21**, 275.
11. Nishida, M., Ohgi, H., Itai, I., Chiba, A. and Yamauchi, K., *Acta mater.*, 1995, **43**(3), 1219.
12. Krishnan, M. and Singh, J. B., *Acta mater.*, 2000, **48**(6), 1325.
13. Knowles, K. M. and Smith, D. A., *Acta metall.*, 1981, **29**, 101.
14. Hane, K. F. and Shield, T. W., *Acta mater.*, 1999, **47**(9), 2603.
15. Ball, J. M. and James, R. D., *Arch. Rat. Mech. Anal.*, 1987, **100**, 13.
16. Gupta, S. P. and Johnson, A. A., *Trans. JIM*, 1973, **14**, 292.
17. Onda, T., Bando, Y., Ohba, T. and Otsuka, K., *Trans. Mater. JIM*, 1992, **33**, 354.
18. Jacobus, K., Sehitoglu, H. and Balzer, M., *Metal. Trans. A*, 1996, **27**, 3066.
19. Gall, K., Sehitoglu, H., Chumlyakov, Y. I., Kireeva, I. V. and Maier, H. J., *J. Eng. Mat. Tech.*, 1999, **121**(1), 19.
20. Surikova, N. S. and Chumlyakov, Y., *Phys. Metals Metal.*, 2000, **89**(2), 196.